17. Brown, A. B. D., Ferrero, C., Narayanan, T. & Rennie, A. R. Phase separation and structure in a concentrated colloidal dispersion of uniform plates. *Eur. Phys. J. B* **11,** 481–489 (1999).
18. Onsager, L. The effect of shape on the interaction of colloidal particles. *Ann. NY Acad. Sci.* **51,** 627–659 (1949).
19. Frenkel, D. & Eppenga, R. Monte Carlo study of the isotropic-nematic transition in a fluid of thin hard disks. *Phys. Rev. Lett.* **52,** 1089–1092 (1982).
20. Bates, M. & Frenkel, D. Nematic-isotropic transition in polydisperse systems of infinitely thin hard platelets. *J. Chem. Phys.* **110,** 6553–6559 (1999).
21. Bates, M. Influence of particle shape on the nematic-isotropic transition of colloidal platelet systems. *J. Chem. Phys.* **111,** 1732–1736 (1999).
22. Guinier, A. *X-ray Diffraction in Crystals, Imperfect Crystals, & Amorphous Bodies* 169–172 (Dover, New York, 1994).
23. van der Kooij, F. M., Philipse, A. P. & Dhont, J. K. G. Sedimentation and diffusion in suspensions of sterically stabilized colloidal platelets. *Langmuir* **16,** 5317–5323 (2000).
24. Bibette, JU. Depletion interactions and fractionated crystallisation for polydisperse emulsion purification. *J. Colloid Interface Sci.* **147,** 474–478 (1991).
25. Smits, C., Briels, W. J., Dhont, J. K. G. & Lekkerkerker, H. N. W. Influence of the stabilizing coating on the rate of crystallization of colloidal suspensions. *Prog. Colloid Polym. Sci.* **79,** 287–292 (1989).
26. van der Kooij, F. M. & Lekkerkerker, H. N. W. The liquid crystalline phase behaviour of a colloidal rod-plate mixture. *Phys. Rev. Lett.* **84,** 781–784 (2000).
27. van Bruggen, M. P. B., Dhont, J. K. G. & Lekkerkerker, H. N. W. Morphology and kinetics of the isotropic-nematic phase transition in dispersions of hard rods. *Macromolecules* **32,** 2256–2264 (1999).
28. Gitzen, W. H. *Alumina as a Ceramic Material* 31 (The American Ceramic Society, Columbus, 1970).

Acknowledgements

We thank A. R. Rennie for discussions concerning the columnar phase, I. Dolbnya and W. Bras for technical support at DUBBLE, and D. Frenkel for a critical reading of the manuscript. This work was supported by the Foundation for Fundamental Research on Matter (FOM) and the Netherlands Organization for the Advancement of Research (NWO).

Correspondence should be addressed to H.L. (e-mail: H.N.W.Lekkerkerker@chem.uu.nl).

Multiscale modelling of plastic flow localization in irradiated materials

Tomas Diaz de la Rubia*, Hussein M. Zbib†, Tariq A. Khraishi†, Brian D. Wirth*, Max Victoria‡ & Maria Jose Caturla*

* *Lawrence Livermore National Laboratory, 7000 East Avenue, L-353, Livermore, California 94550, USA*
† *Washington State University, School of Mechanical & Materials Engineering, Pullman, Washington 99164, USA*
‡ *EPFL-CRPP-Fusion Technology Materials, 5232 Villigen PSI, Switzerland*

The irradiation of metals by energetic particles causes significant degradation of the mechanical properties[1,2], most notably an increased yield stress and decreased ductility, often accompanied by plastic flow localization. Such effects limit the lifetime of pressure vessels in nuclear power plants[3], and constrain the choice of materials for fusion-based alternative energy sources[4]. Although these phenomena have been known for many years[1], the underlying fundamental mechanisms and their relation to the irradiation field have not been clearly demonstrated. Here we use three-dimensional multiscale simulations of irradiated metals to reveal the mechanisms underlying plastic flow localization in defect-free channels. We observe dislocation pinning by irradiation-induced clusters of defects, subsequent unpinning as defects are absorbed by the dislocations, and cross-slip of the latter as the stress is increased. The width of the plastic flow channels is limited by the interaction among opposing dislocation dipole segments and the remaining defect clusters.

The microstructure of irradiated materials evolves over a wide range of length and time scales, making radiation damage an inherently multiscale phenomenon. At the shortest scales (nanometres and picoseconds), recoil-induced cascades of energetic atomic displacements give rise to a highly non-equilibrium concentration of point defects and point defect clusters[5]. Over macroscopic length and time scales these defects can migrate and alter the chemistry and microstructure, often inducing significant degradation of mechanical and other properties[1,2]. In metals, the main features of neutron or ion beam irradiation-induced mechanical behaviour can be summarized as[2]: (1) a sharp increase in yield stress with irradiation dose; (2) the appearance of a yield point followed by a yield drop in f.c.c. metals; and (3) an instability that results in plastic flow localization within 'dislocation channels' and leads to loss of ductility and premature failure. An example of flow localization is shown in Fig. 1 (ref. 6). The transmission electron microscopy image shows a channel where all visible irradiation-induced point defect clusters are absent and where uniform large shear (about 100%) has taken place. The channels are 100 to 200 nm wide. Plastic flow localization is responsible for the observed loss of ductility.

Early theories of irradiation hardening focused on various source and dispersed barrier mechanisms[7,8]. Recently[9,10], the analytical cascade-induced source hardening (CISH) model was proposed[9,10]. This model uses insights from molecular dynamics simulations[11–14] and accounts for some of the recent experimental observations. In the model, it is postulated that interstitial clusters produced in displacement cascades form glissile dislocation loops that migrate in one dimension by thermally activated glide, and decorate dislocations, thereby pinning them. However, while this model provides a rational explanation for the observed increase in yield stress, it does not account for plastic flow localization and the development of plastic instabilities.

Here we couple these experimental and atomistic simulation results[11–18] to a three-dimensional dislocation dynamics (DD) simulation to investigate the relation between the irradiation field and mechanical behaviour. We consider two cases, Cu and Pd, which exhibit different damage morphologies under irradiation. Experiments have shown that vacancy stacking-fault tetrahedra (SFT) are the predominant defect type in low stacking fault energy Cu[6,19], whereas in high stacking fault energy Pd, self-interstitial atom Frank sessile loops constitute the majority of observed defects[20,21]. Our DD simulation box is a cube 5 μm in size that contains an initial density of Frank–Read dislocation sources distributed at random on {111} planes. In our DD simulation[22–24], the plastic deformation of a single crystal is obtained by explicit accounting of the dislocation evolution history, that is, their motion and structure.

The motion and interaction of an ensemble of dislocations in a three-dimensional crystal is marched in time. Dislocations are discretized into straight-line segments of mixed character. The Peach–Koehler force F acting on a dislocation segment inside the computational cell is calculated from the stress fields that are caused by immediate neighbouring segments, all other dislocations segments, all defect clusters and the applied stress. The result is used to advance the dislocation segment based on a linear mobility model, $v_{gi} = M_{gi}F_{gi}$, where v_{gi} is the glide velocity of the dislocation segment, M_{gi} is the dislocation mobility, and F_{gi} is the glide component of the Peach–Koehler force minus the Peierl's friction. On the basis of the history of dislocation motion, we obtain a measure for the macroscopic plastic strain rate. To ensure continuity of dislocation lines across the boundaries, we apply reflection boundary conditions[22]. Due to the long-range character of the dislocation stress field, long-range interactions are computed explicitly[22].

In the simulation, segments that are on the verge of experiencing short-range interactions are identified. Based on a set of physical rules, such reactions may result in the formation of junctions, jogs, dipoles, and so on. The dislocations multiply by a variety of

mechanisms that may involve superjog collisions[25], standard Frank–Read source multiplication, and double cross slip. Cross slip is described as an activated process with probability P given by

$$P = \alpha\Omega_1\delta t \exp\left(-\frac{\Delta W^* - \tau A}{kT}\right) \quad \text{for} \quad \Omega_1 = \frac{C_t\pi}{L}$$

where Ω_1 is the fundamental frequency of a vibrating dislocation segment of length L, C_t is the transverse sound velocity, δt is the time increment, α is a numerical parameter controlling the frequency of cross slip, ΔW^* is the activation energy for cross-slip[23], τ is the resolved shear stress, A is the area swept by the dislocation segment that undergoes cross-slip, k is Boltzmann's constant and T is temperature.

The irradiation field is modelled by mapping into the DD box the spatial distribution of defect clusters (SFT and/or Frank sessile interstitial loops) that results from a particular irradiation fluence, temperature and particle energy. At room temperature, typical defect cluster radii are 0.5 to 3 nm and their density in the bulk, ρ_B, ranges from 10^{21}–$10^{24}\,m^{-3}$, depending on irradiation fluence[17,19,20]. In the simulation, this translated into 100,000 to 2 million defect clusters. Following the CISH model[9,10], Frank–Read sources decorated along the dislocation line with defect clusters are

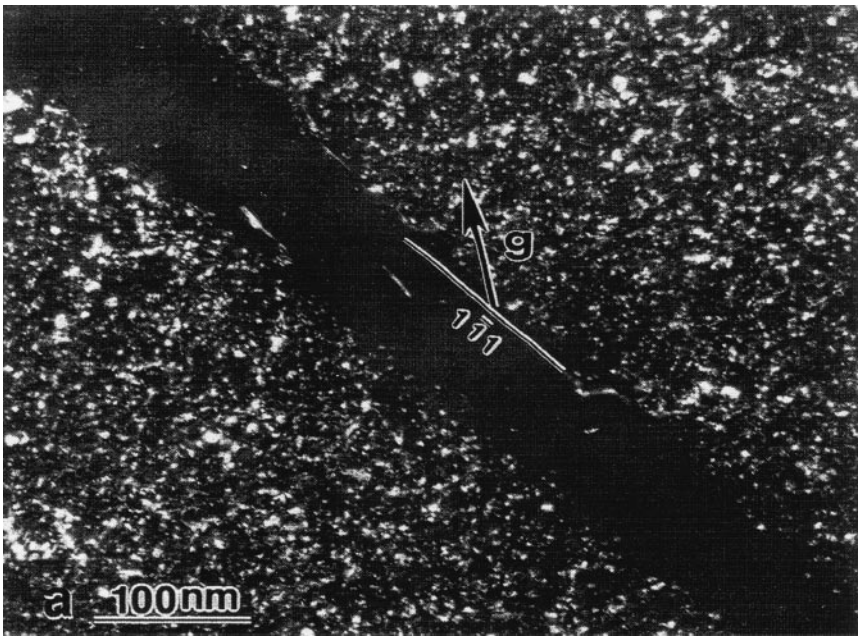

Figure 1 Defect-free channel in deformed irradiated Cu. Weak-beam dark-field transmission electron microscope image shows defect-free channels formed during deformation of Cu irradiated with 600-MeV protons[5].

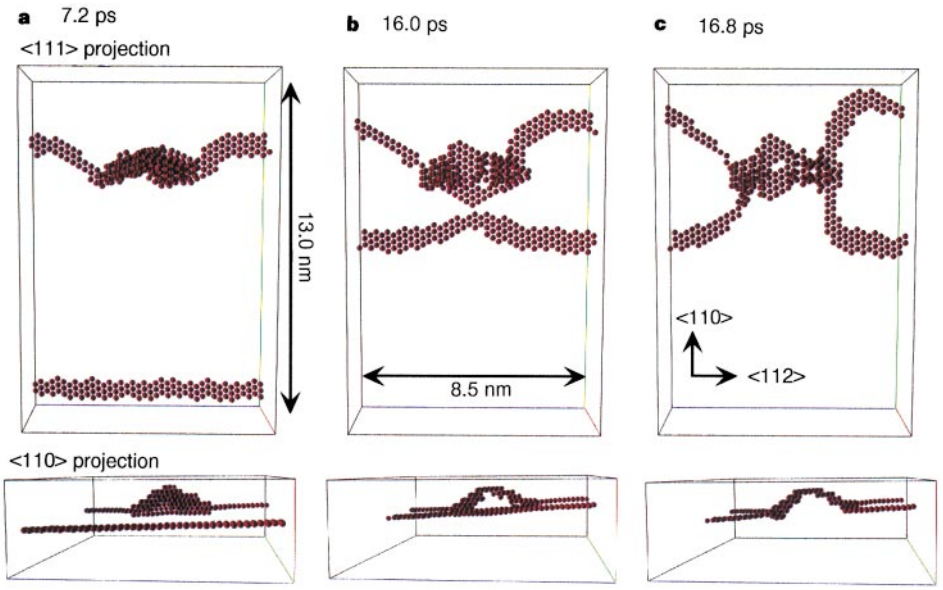

Figure 2 Molecular dynamics simulation of the interaction between an edge dislocation and an overlapping, truncated vacancy stacking-fault tetrahedron (SFT) in Cu. **a**–**c**, ⟨111⟩ (top) and ⟨110⟩ (bottom) projections of high-energy atoms show the motion of two Shockley partial dislocations on their {111} glide plane and their interaction with an overlapping vacancy SFT at **a** 7.2, **b** 16.0 and **c** 16.8 ps after application of a 300-MPa shear stress. A triangular vacancy platelet that is bounded by ⟨110⟩ directions forms a single SFT. A triangular vacancy platelet bounded by two ⟨110⟩ and one ⟨112⟩ directions forms two partial SFTs, one above and one below the initial plane; we define this as an overlapping truncated SFT.

also introduced into the DD simulation as described below.

Dislocation segments interact with the irradiation-induced defect clusters. The elastic interaction of a moving dislocation with a defect cluster (SFT or loop) can be obtained from elasticity theory. However, elasticity calculations cannot by themselves determine the fate of the defect cluster as it interacts with the moving dislocation. To address this point, we have performed molecular dynamics simulations of dislocation–SFT interactions. Figure 2 shows the results of a simulation involving 933,000 atoms at 100 K in Cu. In this simulation, overlapping truncated SFTs (see Fig. 2 legend), such as formed by ageing displacement cascades[17], with a spacing of 8.5 nm (along the dislocation line direction ⟨112⟩) are placed on the glide plane of a dissociated edge dislocation. The two partial dislocations then move under an applied shear stress of 300 MPa. Figure 2a shows that upon contact, the leading partial dislocation is initially pinned by the overlapping SFT. At a later time, Fig. 2b, the leading partial dislocation absorbs part of the overlapping SFT and climbs (clearly seen in ⟨110⟩ projection) as the trailing partial dislocation approaches. Finally, in Fig. 2c, we show that the trailing partial dislocation catches the leading partial dislocation at the location of the overlapping SFT, constricts and climbs by absorbing the remaining defect. Following absorption of the SFT, the dislocation continues to move but with reduced mobility as a result of the jogs that form on the constricted line segment. Although this simulation clearly shows defect absorption, the case is not unique and we are at present investigating the matrix of possible interactions.

For Frank sessile dislocation loops (relevant to Pd), the elastic interaction is computed explicitly[26]. Here the Frank sessile loop is absorbed by the dislocation line if the loop 'unfaults' and becomes glissile. We can calculate the energy difference[27], ΔE, between the faulted loop state and the unfaulted state (that is, a perfect loop), taking into account the interaction energy between the dislocation and the sweeping Shockley partials. When $\Delta E > 0$, the critical radius for loop unfaulting decreases and the loop may transform from the faulted sessile to the unfaulted glissile configuration. When the critical radius for unfaulting is reached, the loop gets absorbed at the core of the dislocation and the dislocation is able to move. Recently, atomistic simulations for interstitial loops consistent with this model have been carried out[28].

Figure 3 shows the stress–strain curves obtained with our DD simulations for Cu irradiated to $\rho_B = 8.24 \times 10^{21}\ m^{-3}$, which considering a uniform defect distribution, corresponds to a SFT spacing of 50 nm. The initial network dislocation density is $\rho_N = 10^{12}\ m^{-2}$. Without irradiation the system yields at about 37 MPa, and work hardening starts at the early stage of deformation as a result of dislocation multiplication and forest interactions. When irradiation-induced defects are present, two behaviours are seen. When the defect density along the line (ρ_D) is such that the average spacing is only 10 nm, that is, $\rho_D \gg \rho_B$, a clear yield point followed by a yield drop can be observed. However, when the average spacing between defects along the dislocation line is 30 nm, which is comparable to that in the bulk, the system yields at a slightly higher stress and only a very diffuse yield drop is apparent. This is in good agreement with experiments[5] which show that the observed yield drop disappears at elevated doses where $\rho_D \approx \rho_B$. The dose dependence of the yield stress obtained in our DD simulations of irradiated Pd (for more details see ref. 29), where all the irradiation-induced defect clusters are Frank sessile dislocation loops, has a slope of 0.35, which is in excellent agreement with experimental observations[21].

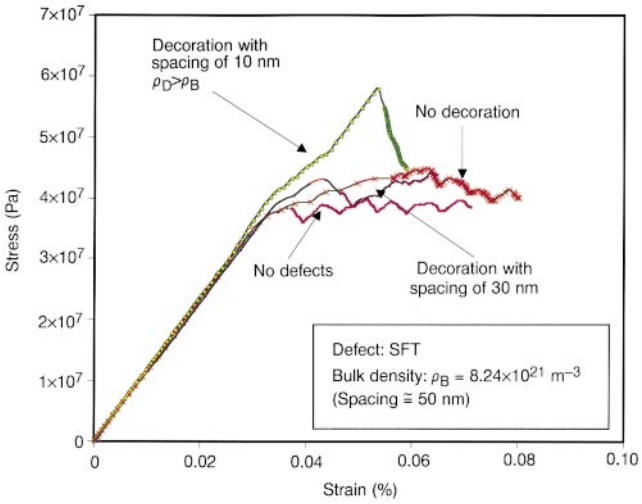

Figure 3 Dislocation dynamics (DD) results of stress–strain curves. Shown are the stress–strain curves obtained with our DD simulations for Cu irradiated to $\rho_B = 8.24 \times 10^{21}\ m^{-3}$. Without irradiation the system yields at about 37 MPa. When the defect density along the line (ρ_D) is such that $\rho_D \gg \rho_B$, a clear yield point followed by a yield drop can be observed. However, when the average spacing between defects along the dislocation line is 30 nm, which is comparable to that in the bulk, the system yields at a slightly higher stress and only a very diffuse yield drop is apparent.

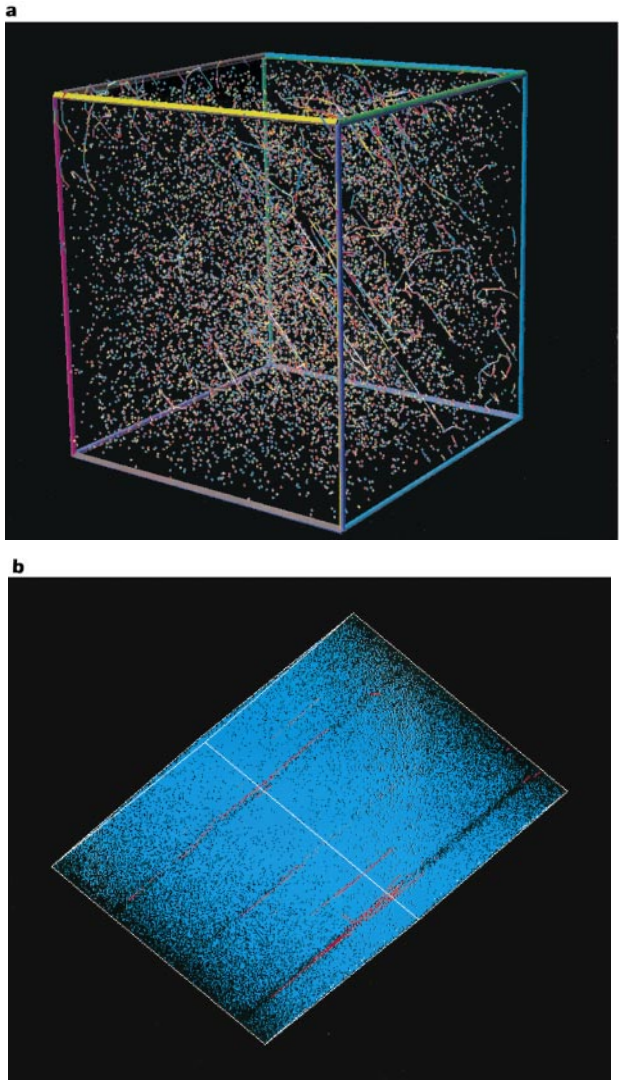

Figure 4 Dislocation dynamics results of channel formation and flow localization. **a**, Results of DD simulation in Cu irradiated to $\rho_B = 8.24 \times 10^{21}\ m^{-3}$ with an initial network dislocation density of $\rho_N = 10^{12}\ m^{-2}$. Shown is the 10-μm side computational cell containing the dislocations and point defects with defect-free channels. **b**, Two-dimensional projection of **a**.

Figure 4a and its projection into two dimensions (Fig. 4b) show the results of our simulations in Cu where cross-slip/double cross-slip takes place and irradiation-induced SFT defects are absorbed by sweeping dislocations based on the criterion discussed above. Figure 4 shows localization of plastic flow in defect-free channels. The channel width is approximately 200 nm with a channel spacing of 1,000 nm in agreement with experimental observations[1]. Examination of the simulation results reveals that the mechanism of channel formation can be described as follows. As dislocations propagate from a Frank–Read source, a screw dislocation segment may be pinned by the defects and eventually cross slip from its primary plane as the stress is increased. This is followed by double cross-slip of the segment, creating a new dislocation source on a parallel plane. This process continues with dislocation segments cross-slipping progressively from one glide plane to another, resulting in a set of parallel planes with active dislocations (the spacing between each pair of planes varies between 25 and 50 nm). Eventually, spreading of the band is limited by the interaction between segments of opposite sign that, in concert with the defects, exerts a backstress on those segments attempting to cross-slip. However, the process is continuous with dislocations being emitted from the same original single source, cross-slipping to adjacent planes and so on, resulting in a large local shear strain (about 100%) in the band. The spacing between the channels is a stochastic variable determined by the spatial distribution of dislocation sources. □

Received 23 February; accepted 30 June 2000.

1. Eyre, B. L. & Barlett, A. F. An electron microscope study of neutron irradiation damage on α-iron. *Phil. Mag.* **12,** 261–271 (1965).
2. Victoria, M. *et al.* The microstructure and associated tensile properties of irradiated fcc and bcc metals. *J. Nucl. Mater.* **276,** 114–122 (2000).
3. Odette, G. R. & Lucas, G. E. Recent progress in understanding reactor pressure vessel steel embrittlement. *Radiat. Effects Defects Solids* **144,** 189–231 (1998).
4. Bloom, E. E. The challenge of developing structural materials for fusion power systems. *J. Nucl. Mater.* **258–263,** 7–17 (1998).
5. Averback, R. S. & Diaz de la Rubia, T. in *Solid State Physics* Vol. 51 (eds Spaepen, F. *et al.* & Ehrenreich, H.) 281–402 (Academic, New York, 1998).
6. Dai, Y. & Victoria, M. Defect cluster structure and tensile properties of Cu single crystals irradiated with 600 MeV protons. *MRS Symp. Proc.* **439,** 319–324 (1997).
7. Friedel, J. *Dislocations* (Pergamon, Oxford, 1964).
8. Bement, A. L. Fundamental materials problems in nuclear reactors. In *Proc. 2nd Int. Conf. Strength of Metals Alloys* Vol. II, 693–728 (The American Society for Metals, 1970).
9. Trinkaus, H., Singh, B. N. & Foreman, A. J. E. Segregation of cascade induced interstitial loops at dislocations: possible effect on initiation of plastic deformation. *J. Nucl. Mater.* **251,** 172–187 (1997).
10. Singh, B. N., Foreman, A. J. E. & Trinkaus, H. Radiation hardening revisited: role of intracascade clustering. *J. Nucl. Mater.* **249,** 103–115 (1997).
11. Diaz de la Rubia, T. & Guinan, M. W. New mechanism of defect production in metals: A molecular-dynamics study of interstitial-dislocation-loop formation in high-energy displacement cascades. *Phys. Rev. Lett.* **66,** 2766–2769 (1991).
12. Foreman, A. J. E., Phythian, W. J. & English, C. A. The molecular dynamics simulation of irradiation damage cascades in copper using a many-body potential. *Phil. Mag. A* **66,** 671–695 (1992).
13. Wirth, B. D., Odette, G. R., Maroudas, D. & Lucas, G. E. *J. Nucl. Mater.* **244,** 185–194 (1997).
14. Osetsky, Y. N., Bacon, D. J. & Serra, A. Thermally activated glide of small dislocation loops in metals. *Phil. Mag. Lett.* **79,** 273–282 (1999).
15. Wirth, B. D., Bulatov, V. & Diaz de la Rubia, T. Atomistic simulation of stacking fault tetrahedra formation in Cu. *Proc. Int. Conf. Fusion Reactor Materials ICFRM-9, J. Nucl. Mater.* (in the press).
16. Heinisch, H. L. Computer simulation of high energy displacement cascades. *Radiat. Effects Defects Solids* **113,** 53–73 (1990).
17. Caturla, M. J. *et al.* Comparative study of radiation damage accumulation in Cu and Fe. *J. Nucl. Mater.* **276,** 13–21 (2000).
18. Soneda, N. & Diaz de la Rubia, T. Defect production, annealing kinetics and damage evolution in alpha-Fe: an atomic-scale computer simulation. *Phil. Mag. A* **78,** 995–1019 (1998).
19. Singh, B. N. & Zinkle, S. J. Defect accumulation in pure fcc metals in the transient regime: a review. *J. Nucl. Mater.* **206,** 212–229 (1993).
20. Baluc, N., Dai, Y. & Victoria, M. Plasticity and microstructure of irradiated Pd. *MRS Symp. Proc.* **540,** 555–560 (1999).
21. Baluc, N., Bailat, C., Luppo, M.-I., Schaublin, R. & Victoria, M. Comparison of the microstructure and tensile behavior irradiated fcc and bcc metals. *MRS Symp. Proc.* **540,** 539–548 (1999).
22. Zbib, H. M., Rhee, M. & Hirth, J. P. On plastic deformation and the dynamics of 3D dislocations. *Int. J. Mech. Sci.* **40,** 113–127 (1998).
23. Rhee, M., Zbib, H. M., Hirth, J. P., Huang, H. & Diaz de la Rubia, T. Models for long/short range interactions in 3D dislocation simulation. *Model. Simul. Mater. Sci. Eng.* **6,** 467–492 (1998).
24. Zbib, H. M., Diaz de la Rubia, T., Rhee, M. & Hirth, J. P. 3D dislocation dynamics: stress-strain behavior and hardening mechanisms in fcc and bcc metals. *J. Nucl. Mater.* **276,** 154–165 (2000).
25. Rhee, M., Lassila, D. H., Bulatov, V. V., Hshuing, L. & Diaz de la Rubia, T. Dislocation multiplication and the early stages of plastic deformation in bcc molybdenum: a dislocation dynamics numerical simulation. *Phys. Rev. Lett.* (submitted).
26. Khraishi, T. A., Zbib, H. M., Hirth, J. P. & Diaz de la Rubia, T. The stress field of a general circular Volterra dislocation loop: analytical and numerical approaches. *Phil. Mag. Lett.* **80,** 95–105 (2000).
27. Ghoniem, N. M., Singh, B. N., Sun, L. Z. & Diaz de la Rubia, T. Interaction and accumulation of glissile defect clusters near dislocations. *J. Nucl. Mater.* **276,** 166–177 (2000).
28. Rodney, D. & Martin, G. Dislocation pinning by small interstitial loops: a molecular dynamics study. *Phys. Rev. Lett.* **82,** 3272–3275 (1999).
29. Khraishi, T. A., Zbib, H. M., Diaz de la Rubia, T. & Victoria, M. Localized deformation and hardening in irradiated metals: 3D discrete dislocation dynamics simulations. *Acta Metall. Mater.* (submitted).

Acknowledgements

This work was performed in part under the auspices of the US Department of Energy by Lawrence Livermore National Laboratory. Work by M.V. was performed under a contract of the Swiss National Research Fund.

Correspondence and requests for materials should be addressed to T.D.R. (e-mail: delarubia@llnl.gov).

A stable argon compound

Leonid Khriachtchev, Mika Pettersson, Nino Runeberg, Jan Lundell & Markku Räsänen

Department of Chemistry, PO Box 55 (A.I.Virtasen aukio 1), FIN-00014 University of Helsinki, Finland

The noble gases have a particularly stable electronic configuration, comprising fully filled *s* and *p* valence orbitals. This makes these elements relatively non-reactive, and they exist at room temperature as monatomic gases. Pauling predicted[1] in 1933 that the heavier noble gases, whose valence electrons are screened by core electrons and thus less strongly bound, could form stable molecules. This prediction was verified in 1962 by the preparation of xenon hexafluoroplatinate, $XePtF_6$, the first compound to contain a noble-gas atom[2,3]. Since then, a range of different compounds containing radon, xenon and krypton have been theoretically anticipated and prepared[4–8]. Although the lighter noble gases neon, helium and argon are also expected to be reactive under suitable conditions[9,10], they remain the last three long-lived elements of the periodic table for which no stable compound is known. Here we report that the photolysis of hydrogen fluoride in a solid argon matrix leads to the formation of argon fluorohydride (HArF), which we have identified by probing the shift in the position of vibrational bands on isotopic substitution using infrared spectroscopy. Extensive *ab initio* calculations indicate that HArF is intrinsically stable, owing to significant ionic and covalent contributions to its bonding, thus confirming computational predictions[11–13] that argon should form a stable hydride species with properties similar to those of the analogous xenon and krypton compounds reported before[14–18].

We prepared hydrogen fluoride in an argon matrix by passing argon over an HF–pyridine polymer (Fluka) at room temperature, and condensing the mixture onto a CsI substrate kept at 7.5 K. The argon used was either ^{40}Ar (100%; AGA) or ^{36}Ar (99.5% isotopically enriched; ICON Services). By optimizing the experimental conditions, fairly monomeric samples of HF were obtained in the matrix (infrared bands corresponding to H–F stretching vibrations were found at $\nu_{HF} = 3{,}962$ and $3{,}954\ cm^{-1}$; $\nu_{DF} = 2{,}895\ cm^{-1}$), as evidenced by comparison with previous HF/Ar matrix-isolation studies[19]. A very high degree of deuteration (> 90%) was achieved by passing the gaseous HF/Ar mixture through a volume containing small amounts of liquid deuterated sulphuric acid.

Photolysis of the HF was performed by illuminating the HF/Ar matrix (through a MgF_2 window) with a Kr vacuum-ultraviolet continuum discharge lamp (Opthos), which emitted in the spectral region of 127–160 nm wavelength. Typically, only a fraction (< 30%) of HF dissociated when this light source was used, even